ICARUS 69, 506–518 (1987)

Impact Experiments in Low-Temperature Ice

MANFRED A. LANGE[1] AND THOMAS J. AHRENS

Seismological Laboratory, California Institute of Technology, Pasadena, California 91125

Received September 3, 1985; revised October 15, 1986

New results of low-velocity impact experiments in cubic and cylindrical (20 cm) water-ice targets initially at 257 and 81°K are reported. Impact velocities and impact energies vary between 0.1 and 0.64 km/sec and 10^9 and 10^{10} ergs, respectively. Observed crater diameters range from 7 to 15 cm and are two to three times larger than values found for equal-energy impacts in basaltic targets. Crater dimensions in ice targets increase slightly with increasing target temperatures. Crater volumes of strength-controlled ice craters are about 10 to 100 times larger than those observed for craters in crystalline rocks. Based on similarity analysis, general scaling laws for strength-controlled crater formation are derived and are applied to crater formation on the icy Galilean and Saturnian satellites. This analysis indicates that surface ages, based on impact-crater statistics on an icy crust, will appear greater than those for a silicate crust which experienced the same impact history. The greater ejecta volume for cratering in ice versus cratering in silicate targets leads to accelerated regolith production on an icy planet.

INTRODUCTION

Voyager observations of the icy satellites of Jupiter and Saturn have revealed that many of their surfaces are dominated by impact craters (e.g., Smith *et al.*, 1979, 1981; Morrison, 1982). Cratered surfaces are also characteristic of at least two of the four terrestrial planets. The major difference, which complicates comparison of cratering phenomena, is the different material responses of icy and silicate crusts. Based largely on the Voyager spacecraft data, we know that the crusts of the icy satellites contain copious amounts of water ice at temperatures between 120 and 70°K (Smith *et al.*, 1979, 1981; Clark, 1982).

A necessary prerequisite to understanding the evolution and the history of the icy planets is knowledge of the pertinent impact mechanics in ice at low temperatures. In contrast to cratering in silicate rocks, which has been studied extensively both via impact and with explosives up to very large sizes (e.g., Roddy *et al.*, 1977), data on impact cratering in ice are scarce and only available for a limited size and energy range (Croft *et al.*, 1979; Croft, 1981; Lange and Ahrens, 1981, 1982a; Kawakami *et al.*, 1983; Cintala *et al.*, 1985). A basic limitation of these experiments lies in the fact that all of these laboratory-sized craters must be regarded as being strength dominated and that most of these craters (except for the present results) were obtained in ice at temperatures higher than appropriate for the icy planets (i.e., mostly at temperatures between ~250 and 260°K).

In the present paper we present cratering data obtained on H_2O ice at 257 and 81°K over a range of energies from $\sim 0.8 \times 10^9$ to $\sim 1.6 \times 10^{10}$ ergs. Generalized scaling relations have been developed using similarity variable analysis which permits the application of laboratory cratering data to the smaller, strength-dominated, natural cratering events (Holsapple and Schmidt, 1982; Housen *et al.*, 1983; Holsapple and Housen, 1985). Using similarity variable scaling analysis, we attempt to relate the present data to planetary cratering.

[1] Now at the Alfred-Wegener-Institute for Polar Research, Columbus Center, D 2850 Bremerhaven, FRG.

0019-1035/87 $3.00

TABLE I[a]

Shot No.	T (°K)	v_i (km/sec)	KE (10^9 erg)	p (kbar)	D_{min} (cm)	D_{max} (cm)	D (cm)	h (cm)	V_c (cm^3)	h/D
				Unconfined						
591	257	0.14	0.78	1.28	7.47	8.56	8.02	1.30	27.0	0.16
593	257	0.16	1.05	1.51	7.84	9.94	8.89	1.56	49.8	0.18
602	257	0.21	1.71	1.96	9.79	11.85	10.82	1.33	44.0	0.12
				Confined						
610	257	0.23	2.07	2.17	8.23	11.50	9.71	1.50	56.3	0.15
615	257	0.32	4.27	3.27	10.78	12.90	12.00	2.18	110.7	0.18
618	257	0.27	2.81	2.64	8.93	11.30	9.94	1.72	60.1	0.17
619	257	0.50	9.95	5.44	13.14	17.78	15.46	3.72	386.3	0.24
608	81	0.24	2.37	2.34	6.37	9.51	8.12	1.49	28.2	0.18
613	81	0.34	4.85	3.52	7.54	11.71	10.13	2.00	61.9	0.20
616	81	0.20	1.62	1.91	6.76	7.70	7.24	1.20	20.0	0.17
617	81	0.23	2.23	2.26	6.11	9.28	7.57	1.15	19.5	0.15
849	81	0.64	16.49	7.43	11.8	15.5	14.21	2.2	132.6	0.16
851	81	0.46	8.53	4.96	11.9	13.1	12.50	1.8	115.9	0.14
853	81	0.37	5.52	3.83	8.9	11.7	10.6	1.2	63.9	0.10
855	81	0.31	3.86	3.12	7.5	10.1	8.9	0.9	24.9	0.10

[a] Target temperature T; impact velocity v_i; impact energy KE; peak one-dimensional pressure p; minimum, maximum, and mean crater diameters D_{min}, D_{max}, and D, respectively; crater depth h; crater volume V_c; and crater depth to diameter ratio in experiments h/D.

EXPERIMENTAL TECHNIQUES

Impact experiments were performed on cubic (19 cm length) and cylindrical (diameter, 20 cm; height, 20 cm) water-ice targets at 257 and 81°K. These were impacted in both confined and unconfined target blocks. Cubic targets at 257°K were removed from their plastic molds. For the cylindrical targets at 257 and 81°K, only the bottom of the mold was removed leaving a brass sleeve (~0.64 cm thick) around the target during the impact. Similar techniques were used in preparing the ice targets as described in Lange and Ahrens (1981). Lexan (polycarbonate plastic) projectiles having a density of 1.1 g/cm^3 and a mass of 8 g were launched with a 20-mm chemical propellant gun to velocities between 0.15 and 0.64 km/sec and horizontally impacted the targets. Impact energies ranged from 0.78 to 16.49 $\times$ 10^9 ergs. Experimental parameters are given in Table I.

After each impact, the cratered targets were photographed and the major dimensions of the crater were measured (Table I). The values for the rim diameter D in Table I are the means of four to six measurements of which D_{min} and D_{max} are the minimum and maximum, respectively. Hence, D is not necessarily the mean of D_{min} and D_{max}. The crater depth is the distance between the deepest point inside the crater to the original target surface. The crater volume V_c was determined by filling the crater with fine-grained sand (mean grain size, 0.1 mm) to the level of the original target plane, weighing the used sand, and dividing the weight with the bulk sand density (1.4 g/cm^3). The crater volumes are measured to within $\pm$ 2 cm^3 by this method.

Each impacted target block was subsequently cut open. This allowed inspection of cross sections of the block for impact-induced internal fracture patterns.

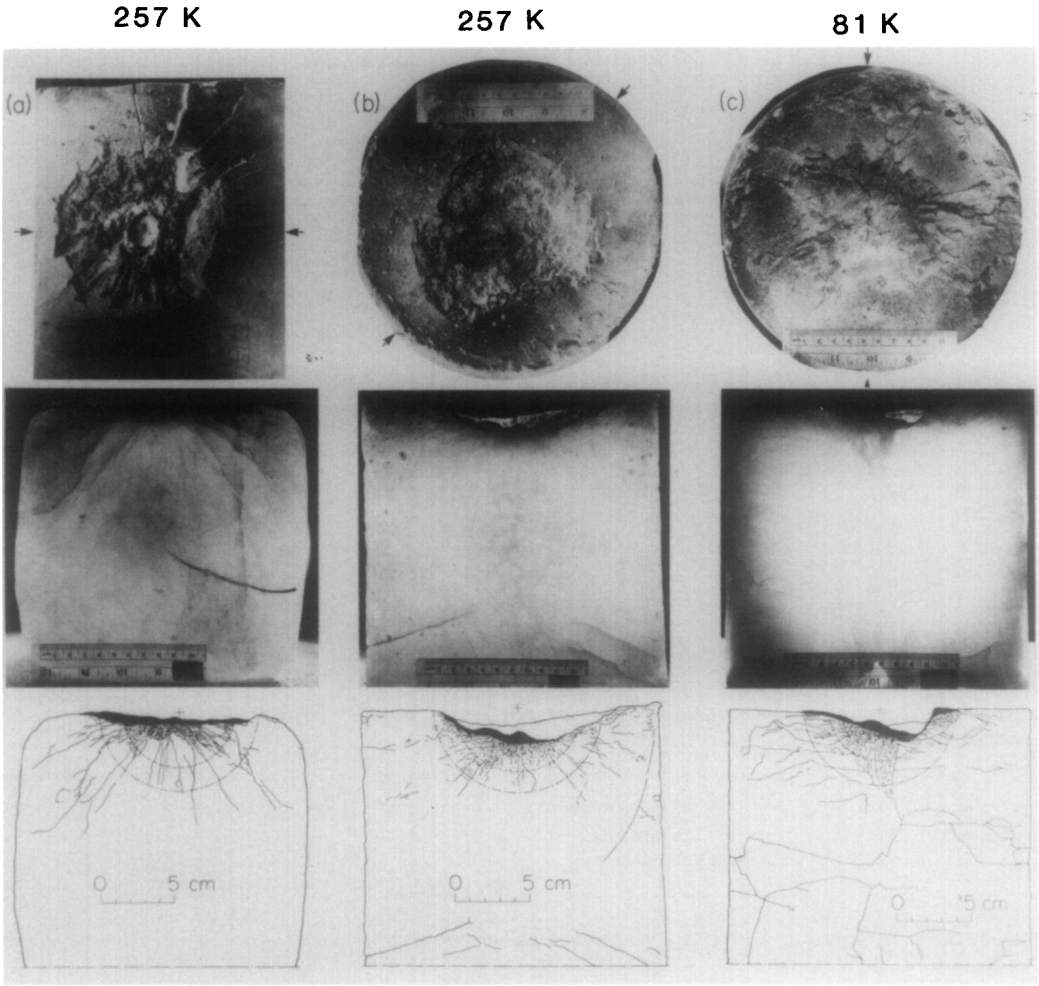

FIG. 1. Impact craters in ice at 257 and 81°K. Shown are top views of the cratered surfaces, cross sections taken in the directions indicated by the arrows in the top photos, and schematic cross sections showing major crack patterns. (a) 257°K, unconfined; (b) 257°K, confined; (c) 81°K, confined.

RESULTS

Major results of the experiments are given in Table I. The one-dimensional peak stresses p, of Table I, are determined by the impedance matching technique using equation of state data of ice I at 263°K (Ahrens and O'Keefe, 1985) and Lexan (Carter and Marsh, 1980).

(1) *Crater Shape and Morphology and Internal Fracture Patterns*

The shapes of the experimental craters in water ice are, in general, highly irregular. Figure 1 shows examples of craters in each of three experimental classes. These are (a) unconfined at 257°K, (b) confined at 257°K, and (c) confined at 81°K. It can be seen that the crater shapes are in most cases (but primarily for the 257°K shots) determined by the spallation of target fragments along radial fractures (surfaces which include radius vectors) centered at the impact point. Intersection of radial with concentric fractures (Surfaces orthogonal to radius vectors) leads to the breakup of larger frag-

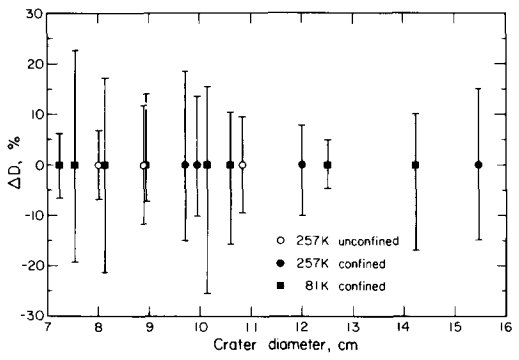

FIG. 2. Minimum, maximum, and mean values of impact crater diameters for different target temperatures.

ments and results in mean sizes of ejected particles generally not exceeding ~1 cm for the experiments of 257°K and ≤0.5 cm for the 81°K targets. Target confinement generally prohibits the formation of cracks originating at the edge of the target block (see Fig. 1a). There is an apparent slight increase of crater shape irregularity in going from unconfined 257°K targets to confined 257°K targets to confined 81°K targets in Fig. 1. However, a plot of the mean crater diameter D versus the differences between minimum and maximum mean diameters $(D - D_{min})/D$ and $(D_{max} - D)/D$, respectively (both terms are plotted as ΔD in Fig. 2), demonstrates that ΔD. D, and the target temperature are independent. The three largest values for ΔD are found for craters in confined 81°K targets.

The interior morphology of each crater is generally very rugged and highly irregular. Almost all of the experimental craters have what appears to be a "central peak" or "central pit" (at the point where the projectile hit the target (Fig. 1)). By "central pit," we refer to a near-circular feature which has a diameter close to the projectile diameter. This strongly suggests a genetic relationship between the pit and the initial projectile impact. It seems that the initial highly compressed target material is not removed by subsequent tensile stresses, which might otherwise lead to failure of the target and excavation.

The fracture pattern at the impacted target surface and inside the target resembles that found in experimental craters in rock (e.g., Hörz, 1969). The uppermost layer of strongly fractured target material and crushed (powdered) ice is seen as the black areas in the photographs of the ice-target cross sections in Fig. 1. We find essentially four types of fractures in the target blocks: radial, concentric, and spall fractures (in all target types), and cracks not related directly to the crater but subparallel to the near-target surface. The latter are evident for confined 81°K targets (Fig. 1c). The radial fractures extend in most cases to the edges of the ice targets (or, alternatively, originate at the edge of the block in the case of the unconfined targets) and are best developed in the unconfined 257°K targets where they represent the major fracture type.

Concentric fractures are prominent in the confined targets at all target temperatures. They have radii reaching the value of the target block radius. Spall fractures can be seen in all ice targets, most clearly in the confined 257°K targets which also show in some cases incipient spallation of target portions on the surface opposite the impact point (back spallation); in only one target, No. 610, back spall failure was actually observed.

Dashed–dotted circles in the cross sections of Fig. 1 mark hemispheric portions of the target with radius equal to $D/2$ and the limit of intense fracturing. It can be seen that these circles enclose most of the fractures induced by the impact. In positioning the inner circles, we attempted to include most of the highly fractured material (mean crack lengths, millimeters to centimeters). The ratios between the radius of the inner hemisphere to that of the outer hemisphere $(D/2)$ and are equal to approximately 0.7 for the unconfined and confined 257°K targets and the confined 81°K target shown in Fig. 1, respectively, and are probably

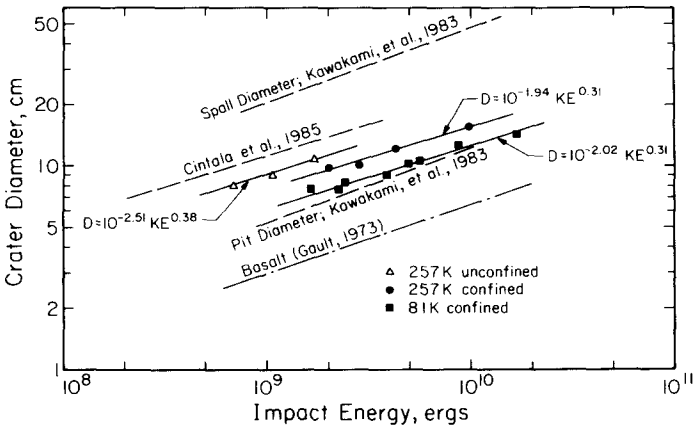

FIG. 3. Crater diameter as a function of impact (projectile kinetic) energy for cratering in ice. For comparison, the data of Kawakami *et al.* (1983) and Cintala *et al.* (1985) are shown together with results for cratering in basalt as given by Gault (1973).

related to stress wave attenuation in the targets.

(2) Crater Dimensions

(a) Crater diameter. Figure 3 shows the relation between mean crater diameter D and impact energy KE for the present experiments. Also given are results for cratering experiments for ice reported by Kawakami *et al.* (1983) and Cintala *et al.* (1985) and for basalt by Gault (1973). In comparing the present results with those of Croft (1981) (not shown), we note that Croft's impact velocities cover a much wider range, reaching a maximum of 6.2 km/sec. The general agreement between all of Croft's data and the present results indicates that the crater size is not very sensitive to impact velocity, at least not in the energy range of Croft's (1981) and the present experiments ($\sim 5 \times 10^8$ to 10^{10} ergs). The spall diameters of both Kawakami *et al.* (1983) and of Cintala *et al.* (1985) lie significantly above the present results, while the pit diameters of Kawakami *et al.* (1983) are in the range of those found in the present 81°K targets.

It can be seen that the crater diameters in the present ice targets lie at about a factor of 2 to 3 above the equal energy values for basaltic targets. This is an important but expected result since the quasi-static compression and tensile strength for basalt (typical values lie at ~3 kbar; Handin, 1966) and ice at 213°K (70 and 30 bar for crushing and tensile strength, respectively; Hobbs, 1974) differ by about two orders of magnitude. Least-squares fits to our data were used to determine the constants a_D, b_D in

$$\log D = a_D + b_D \log KE \qquad (1)$$

which are given in Fig. 3. As can be seen, while the slopes (i.e., b_D) of the diameter versus energy relations are very similar for each of our target types, the crater diameter for a particular impact energy is largest for unconfined ice targets at 257°K and slightly less for confined 257 and 81°K targets. Hence, the crater diameter seems to depend on both target confinement and target temperature. We have adopted a single mean value of the slope for the energy–crater diameter relation of 0.33. This value agrees with the value for cratering in basalt (0.370; Gault, 1973) and sand (0.376; Moore, 1976). Its reciprocal equals 3.00 and coincides with a value of 3 expected theoretically for strength-dominated crater formation (Gault *et al.*, 1975).

(b) Crater depth versus crater diameter.

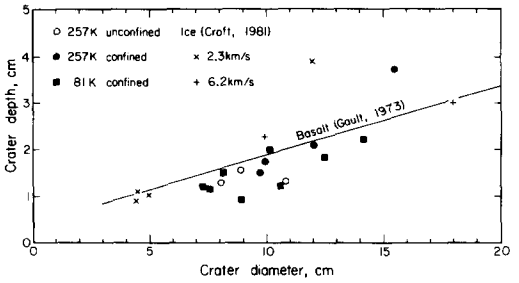

FIG. 4. Crater depth versus crater diameter for experimental impact craters in ice. Results for basalt (Gault, 1973) are also shown.

Values of crater depth versus diameter in our experiments are given in Fig. 4. Also shown is the relation between depth and diameter for basaltic targets from Gault (1973). Although the present data show a relatively large scatter, they generally follow the same trend seen in basaltic craters. However, it appears that craters in ice are slightly shallower than their basaltic counterparts for a given diameter; out of 15 data points for ice craters, 13 lie below the line for craters in basalt. There is no clear correlation of depth to diameter ratio with target type or target temperature.

We interpret the results described above and in the previous section to imply that the diameters of the present experimental craters in ice (at least in the case of the 257°K targets) are mainly spall induced. We further conclude that the crater depths are primarily controlled by projectile penetration. Since these processes in turn depend on dynamic strengths of the target, we conclude that strength of ice increases with decreasing temperature, a result in qualitative agreement with results of a number of quasistatic experiments described by Hobbs (1974), as well as results given by Parameswaran and Jones (1975).

(*c*) *Crater volume.* As a result of ice craters having large diameters, the result shown in Fig. 5 that impact craters in ice have volumes one to two orders of magnitude greater than craters in basalt for a given impact energy is expected. Slopes for the crater volume versus energy relations are similar for ice and basalt. The parameters a_v and b_v in

$$\log V_c = a_v + b_v \log KE \qquad (2)$$

are obtained by least-squares fits to our data (unconfined 257°K targets are excluded from the analysis because of the unusually shallow crater 602) and are given in Fig. 5.

(*d*) *Discussion of results on crater dimension.* Although differences in sample preparation methods affect the actual strength of targets used for ice cratering research, we believe that the data of Croft (1981), the pit-diameter data of Kawakami *et al.* (1983), and the present results can be used as a combined data set to estimate the effect of temperature on cratering efficiencies.

Since our 81°K data fall close to the pit-diameter data of Kawakami *et al.* (1983), we infer that target temperature, although significant, is not a critical parameter in defining cratering efficiencies in ice. However, this contradicts the results of Parameswaran and Jones (1975). They found a

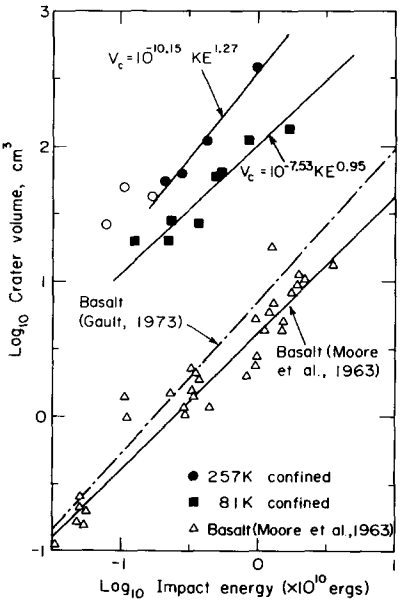

FIG. 5. Crater volume versus impact energy for impact in ice and basalt (Gault, 1973; Moore *et al.*, 1963).

clear increase in the strength of ice with decreasing temperatures, down to 80°K in quasi-static experiments. Our data alone agree with this conclusion, but we are presently not able to rule out the possibility that differences in sample preparation between our and other laboratories might have influenced the targets strong enough to prevent recognition of a more significant temperature effect.

SCALING LAWS FOR LABORATORY CRATERING

(*a*) *The strength-dominated regime.* In the following we attempt to generalize our findings in terms of dimensional and nondimensional scaling laws. Recently, Mizutani *et al.* (1983) proposed a scaling of laboratory-produced craters up to the dimensions of larger, natural, strength-dominated cratering events by defining a "late-stage effective energy," LE:

$$LE = \tfrac{1}{2}mv(C_0 + \tfrac{1}{2}sv). \tag{3}$$

Here, m and v are projectile mass and velocity, and C_0 and s are material parameters relating shock-wave velocity U_s to particle velocity U_p in the target:

$$U_s = C_0 + sU_p. \tag{4}$$

C_0 and, for temperate ice, s are given by Ahrens and O'Keefe (1985) as 1.317 km/sec and 1.526, respectively. Equations (3) and (4) relate the energy coupled or delivered to the target in terms of the target Hugoniot parameters. If crater dimensions are directly related to LE, then planetary gravity does not enter, and we are dealing with a strength-controlled phenomenon. When plotted on a log–log scale, values of LE versus crater diameter D allow specification of a strength-controlled scaling law of the form

$$D = 10^a LE^b. \tag{5}$$

Figure 6 gives LE versus D values of the present experiments (only the confined targets are included in this and the following analysis) and scaling laws in the form of Eq. (5) for the 257 and 81°K targets. Also shown is the relation between LE and the pit-diameter obtained by Kawakami *et al.* (1983). Kawakami *et al.* (1983) find that $b = \frac{2}{5}$ fits their pit-diameter data for ice. Our values of $b \sim \frac{1}{2}$ suggest that with increasing dependence of final crater diameters on strength, which is not explicitly addressed by the "late-stage effective energy," the value of b increases. Kawakami *et al.* (1983) use this relation between D and LE to devise scaling laws applicable to cratering on Mimas and Callisto.

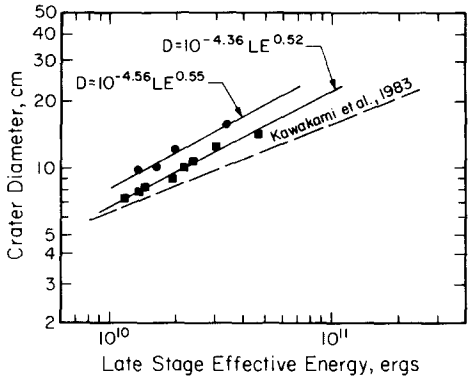

FIG. 6. Late-stage effective energy versus crater diameter for experimental craters in ice. Also shown are results of Kawakami *et al.* (1983) for pit diameters.

(*b*) *Similarity variable scaling.* Using the similarity variable analysis of rock and ice cratering data, Holsapple and Schmidt (1982) and Holsapple and Housen (1986) define cratering efficiency as

$$\pi_v = \frac{V_c\rho}{m} \tag{6}$$

and the scaled crater radius

$$\pi_r = r\left(\frac{\delta}{m}\right)^{1/3} \tag{7}$$

where V is crater volume, m is projectile (impactor) mass, and ρ and δ are target and impactor densities, respectively. They also define the following independent nondimensional (pi) groups:

TABLE II

DIMENSIONAL AND SIMILARITY-SCALED CRATERING DATA

Shot No.	V_i (km/s)	r (cm)	V_c (cm^3)	LE (10^{10} erg)	π_v[a]	π_r[a]	($\pi_2 \times 10^6$)[b]	($\pi_3 \times 10^{-1}$)[c]	Temperature (°K)
610	0.23	4.9	56.3	1.38	6.41	2.38	7.15	2.87	257
615	0.32	6.0	110.7	2.01	12.61	2.91	3.69	1.48	257
618	0.27	5.0	60.1	1.66	6.85	2.42	5.19	2.08	257
619	0.50	7.7	386.3	3.42	44.00	3.73	1.51	0.61	257
608	0.24	4.1	28.2	1.45	3.21	1.99	6.57	5.28	81
613	0.34	5.1	61.9	2.16	7.05	2.47	3.27	2.63	81
616	0.20	3.6	20.0	1.18	2.28	1.75	9.46	7.60	81
617	0.23	3.8	19.5	1.38	2.22	1.84	7.15	5.74	81
849	0.64	7.1	132.6	4.56	15.10	3.44	0.92	0.74	81
851	0.46	6.3	115.9	3.09	13.20	3.05	1.79	1.44	81
853	0.37	5.3	63.9	2.38	7.28	2.57	2.76	2.22	81
855	0.31	14.5	24.9	1.94	2.84	2.18	3.94	3.16	81

[a] $\rho = 0.917$ g/cm^3, $m = 8.05$ g.
[b] $a = 1.20$ cm, $\delta = 1.119$ g/cm^3.
[c] $Y(257°K) = 170$ bar, $Y(81°K) = 340$ bar.

$$\pi_2 = \frac{2g(m/\delta)^{1/3}}{v_i^2} = 3.22\,\frac{ga}{v_i^2} \tag{8}$$

$$\pi_3 = \frac{Y}{\delta v_i^2} \tag{9}$$

where v_i is impact velocity, g is surface gravity, and δ and a are projectile (impactor) density and equivalent radius, respectively. Also, Y is some measure of target strength. Based on experimental data, relations between cratering efficiency π_v and π_2 for gravity-dominated cratering or π_3 for strength-dominated cratering can be defined by

$$\pi_v \pi_2^{\alpha} = A \tag{10}$$

$$\pi_v \pi_3^{\beta} = B \tag{11}$$

where A, B, α, and β, are experimentally derived parameters. Table II gives values of τ_v, π_r, π_2, and π_3, together with values of LE for the present experiments. Figure 7 and 8 show π_v versus π_2 and π_3, respectively, as well as appropriate scaling laws. Also given in Table II are the values of the appropriate constants needed to compute the particular π groups. The strength value Y for 257°K ice is given by Lange and Ahrens (1982b) as the dynamic tensile strength of ice. The value of Y for 81°K ice is chosen to be twice as large as Y for 257°K ice based on results given by Ashby and Frost (1975) and Parameswaran and Jones (1975).

Relation (10) is the most useful one with respect to crater scaling because once A

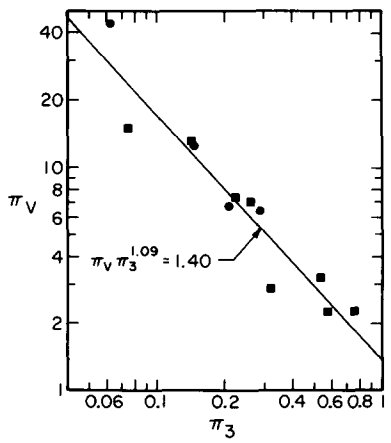

FIG. 7. π_v versus π_3 for craters in ice. Strength Y was chosen to be 170 bar for 257°K ice (Lange and Ahrens, 1982b) and to be 340 bar for 81°K ice.

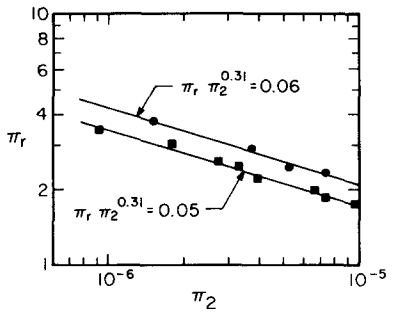

FIG. 8. π_r versus π_2 for cratering data in ice.

and α have been established, V_c can be obtained by the following expression:

$$V_c = \frac{m}{\delta}\left[3.22\,\frac{ga}{v_i^2}\right]^{-\alpha} A. \qquad (12)$$

The use of relations between π_r (Eq. (7)) and π_2 allows direct scaling of crater diameter D via

$$D = 2r = 2\left(\frac{m}{\delta}\right)^{1/3}\left[3.22\,\frac{ga}{v_i^2}\right]^{-\gamma} C \qquad (13)$$

based on a suitable scaling law of the form

$$\pi_r \pi_2^{\gamma} = C. \qquad (14)$$

We explicitly note that Eqs. (10), (12), (13), and (14) are generally valid only when special conditions apply. In general, cratering efficiency π_v depends on both π_2 and π_3, i.e.,

$$\pi_v = f(\pi_2,\pi_3) \qquad (15)$$

where the functional relationship depends on the considered materials and processes. For small-scale cratering, gravity becomes less important and cratering efficiency depends mainly on π_3:

$$\pi_v \simeq f(\pi_3).$$

Large-scale cratering, where most of the energy is expended in lifting and moving the ejecta material, depends mainly on π_2, and π_3 becomes less important:

$$\pi_v \simeq f(\pi_2).$$

It is this case which allows application of the above-mentioned equations.

While our experiments should clearly be regarded as strength dominated, Fig. 7 shows a good fit between π_v and π_2, which demonstrates that projectile velocity scales similar for π_2 and π_3. In this case, π_2 and π_3 are no longer independent and are related by (Eqs. (8) and (9))

$$\pi_3 = [Y/(3.22\delta ag)]\pi_2 \qquad (16)$$

Figure 8 gives π_2 versus π_r values for the present data and scaling of the form of Eq. (14) for 257 and 81°K ice. As can be seen, the π_2 versus π_r data can be very closely fit by linear relations between log π_2 and log π_r. We also note the equivalence between the γ values for 257 and 81°K ice and the fact that $\gamma = \alpha/3$ for 81°K ice, in agreement with theoretical predictions.

In the following, we will estimate the boundaries for application of scaling laws (Eqs. (12) and (13)) based on the present laboratory data.

SCALING LAWS FOR NATURAL CRATERING EVENTS

(1) General

Laboratory experiments generally provide the data necessary to compute α, β, γ, A, B, C in the general scaling laws given in Eqs. (10), (11), and (14), which can be used in their dimensional form (Eq. (15)) to directly relate dependent and independent cratering parameters.

Holsapple and Housen (1986) give an extensive review of existing laboratory and field data on ice cratering. The basic difficulty with the small-scale, low-velocity laboratory cratering experiments lies in the fact that they are strength dominated, and it cannot be conclusively determined whether or not and to what extent they obey rate-dependent strength scaling laws.

In light of their study, we conclude that the data base for the 81°K ice, which we have extended beyond earlier reports (cf. Lange and Ahrens, 1982a), allows scaling laws to be derived for strength-dominated

cratering at low temperatures as occurs on the Galilean and Saturnian satellites.

Relations between dependent and independent π groups for 81°K ice are

$$\pi_v \pi_3^{1.09} = 1.40 \quad (17)$$

$$\pi_r \pi_2^{0.31} = 0.05 \quad (18)$$

(see Figs. 7 and 8).

(2) Cratering on the Galilean and Saturnian Satellites

Based on scaling relations (17) and (18) and on the range of π_3,

$$5 \times 10^{-2} \leq \pi_3 \leq 10^0, \quad (19)$$

we can now apply the explicit scaling laws (Eqs. (12) and (13)) to cratering events on the icy Galilean and Saturnian satellites given a strength value Y for the target material (here assumed to be 340 bar; see above) and the density of the impactor δ (we consider both icy and silicate impactors with densities of ~1 and ~3 g/cm^3, respectively). Equations (19) and (9) allow specification of permissible impact velocities to be used in the present scaling:

$$0.2 \text{ km/sec} \leq v_i \leq 0.8 \text{ km/sec} \quad (20)$$

for ice impactors and

$$0.1 \text{ km/sec} \leq v_i \leq 0.5 \text{ km/sec} \quad (21)$$

for silicate impactors. These velocities lie below estimates of ~12 to 25 km/sec for cratering on the Jovian and Saturnian satellites (Shoemaker and Wolfe, 1982).

The limits in impact velocity ((20) and (21)) are used to infer limiting impactor sizes, a, to be used in the present scaling based on Eq. (8). Depending on surface gravity, g, we find

$$0.01 \text{ (m/sec)}^2 \leq ga \leq 2.0 \text{ (m/sec)}^2 \quad (22)$$

for ice impactors and

$$2.8 \times 10^{-3} \text{ (m/sec)}^2 \leq ga \leq 0.8 \text{ (m/sec)}^2 \quad (23)$$

for silicate impactors.

We now apply Eqs. (12) and (13) to compute crater volume and crater diameter as a function of impactor size for impact velocities between 0.5 and 10 km/sec. We barely exceed the limits of our scaling laws and note that the results for the higher velocities are of limited reliability. In order to describe cratering counts on the Galilean and Saturnian satellites, surface gravities of 0.1, 0.25, and 1.3 m/sec^2 are assumed, corresponding to Mimas, Enceladus, and Tethys ($g \sim 0.1$); Dione, Rhea, and Iapatus ($g \sim 0.25$); and Europa, Ganymede, and Callisto ($g \sim 1.3$). Figures 9a and 9b give the results for $g = 0.1$ and 1.3. For comparison, relations between π_v and π_2 for water and dry sand as given by Chapman and McKinnon (1985) were used to predict crater volumes in sand and water for impacts of ice projectiles at $v_i = 10$ km/sec. Moore *et al.* (1963) give crater volumes as a function of projectile energy for 31 experiments in basaltic targets. These results can be used to derive a linear relation of the type of Eq. (2) with $a_v = -9.107$ and $b_v = 0.976$. A slightly different form of such a relation,

$$V_c = 10^{a_v} KE^{b_v} = A_v(\tfrac{1}{2}mv_i^2)^{b_v} \quad (24)$$

can be compared with relation (10): $\pi_v \pi_2^\alpha = A$. Using the definitions of π_v and π_2, it follows that

$$\frac{V_c \rho}{m} = A\left[\frac{2g}{v_i^2}\left(\frac{m}{\delta}\right)^{1/3}\right]^{-\alpha},$$

which can be applied to give

$$V_c = A\frac{\delta^{\alpha/3}}{\rho} m^{1-(4/3)\alpha} g^{-\alpha}(\tfrac{1}{2}mv_i^2)^\alpha. \quad (25)$$

Comparison of (24) and (25) yields

$$A = A_v\left[\frac{\delta^{\alpha/3}}{\rho} m^{1-(4/3)\alpha} g^{-\alpha}\right]^{-1} \quad (26)$$

and

$$\alpha = b_v. \quad (27)$$

Thus we can derive A and α from a_v and b_v and obtain

$$\pi_v \pi_2^{0.98} = 1.74 \times 10^{-6}$$

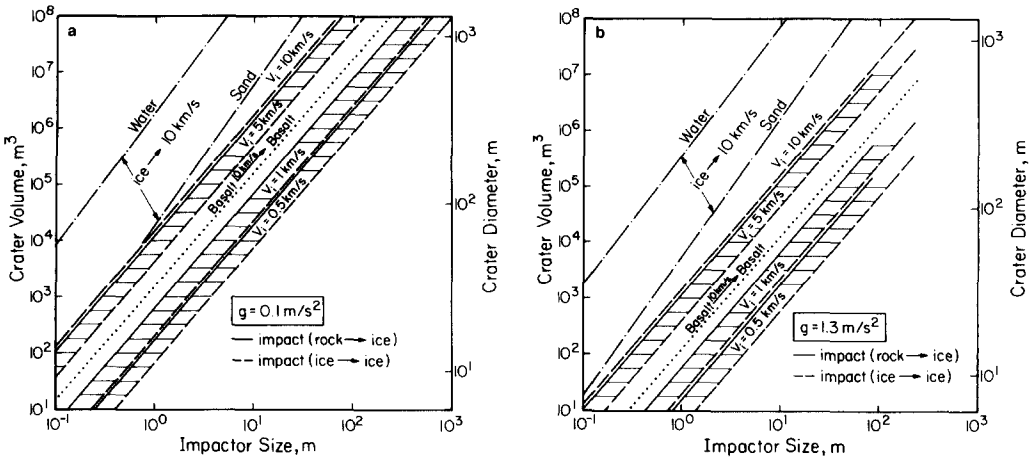

FIG. 9. Crater volume and crater diameter as a function of impactor size for ice targets impacted by ice and rock projectiles. Crater volumes and diameters for impacts of ice into water and dry sand, and impacts of basaltic projectiles onto basalt targets are also shown. Planetary gravities for 0.1 m/sec^2 (a) and 1.3 m/sec^2 (b).

for cratering in basaltic targets. Then again, we note that the above deviation is not strictly correct because the data are mainly strength dominated and application of π_v π_2 relations are not fully appropriate.

The slight discrepancies seen when computed values of A and, α, the exponent for the present ice targets are compared with those values found in linear-regression fits between π_v and π_2 of the present experiments from Eq. 10, versus Eq. 26 due to numerical truncation errors.

We can also give crater volumes for basalt targets being impacted by basalt projectiles at velocities of 10 km/sec (Fig. 9). As can be seen, while craters in cohesionless sand are slightly larger than craters in ice (keeping all other parameters the same), volumes of craters formed in basaltic targets are about a factor of 10 lower than those found in ice (cf. Fig. 5).

DISCUSSION AND CONCLUSIONS

As shown in Fig. 9, the major conclusion to be drawn from the present study is that cratering efficiencies are significantly enhanced in icy targets as compared to their rocky counterparts. This has two important implications.

For a given series of impacting objects with a given size distribution, this will yield a distribution of resulting cratering sizes significantly shifted toward larger craters on icy crusts as compared with rocky (or basaltic) crusts. Thus, relative ages of planetary surfaces based on crater size-frequency distributions will yield apparent older ages of ice surfaces than those obtained for basaltic crusts. This conclusion must be qualified by the following. The present results are strictly valid only for crater formation which involves at least some target strength effect. Holsapple and Housen (1985) place the boundary between strength-dominated and gravity-dominated crater formation at a crater radii of about 10^3 m. Even though the results in Fig. 9 do not exceed this range, we expect that craters of diameters larger than $\sim 10^2$ m should show only a minor strength effect. In the gravity regime, it is only the velocity and density difference between the projectile and target material which is expected to control the final crater size at a fixed planetary gravity.

Of greater importance are the observed crater volumes in ice targets which are approximately a factor of 10 greater than

those in basaltic targets. This will result in accelerated growth of a planetary regolith on icy planets relative to silicate planets. Several authors (e.g., Passey and Shoemaker, 1982; Shoemaker *et al.* 1982) have pointed out the possible importance of a thick regolith layer on the thermal regime of crusts of the icy Galilean and Saturnian satellites. The resulting thermal insulation will lead to a lower viscosity of the crusts or lithospheres of these objects which are expected to induce enhanced relaxation of the craters. Modeling the thermal and relaxation histories of craters on a regolith-covered icy satellite surface needs to be carried out.

ACKNOWLEDGMENTS

We appreciate the assistance of M. Long, E. Gelle, and C. Manning with the experiments. We appreciate both the advice and generous use of the cold-room facility proffered by B. Kamb. The prepublication results provided by K. Holsapple and K. Housen were helpful. M. A. Lange was partly supported by a stipend of the Deutsche Forschungsgemeinschaft. We appreciate helpful comments of S. Croft and K. Holsapple on this paper, which was supported under NASA Contract, NGL 105-002-105, Contribution No. 4268, Division of Geological and Planetary Sciences, California Institute of Technology.

REFERENCES

AHRENS, T. J., AND J. D. O'KEEFE (1985). Shock vaporization and the accretion of the icy satellites of Jupiter and Saturn. In *Ices in the Solar System* (P. Klinger, A. Dollfus, and R. Smoluchowski, Eds.), pp. 631–654. Reidel, Dordrecht.

ASHBY, M. F., AND H. J. FROST (1975). The kinetics of inelastic deformation above 0°K. In *Constitutive Equation in Plasticity* (A. S. Argon, Ed.). MIT Press, Cambridge, MA.

CARTER, W. J., AND S. P. MARSH (1980). Hugoniot equations of state and polymers. In *LASL Shock Hugoniot Data* (S. P. Marsh, Ed.). Univ. of California Press, Berkeley.

CHAPMAN, C. R., AND W. B. MCKINNON (1985). Cratering of planetary satellites. In *Natural Satellites* (J. Burns and D. Morrison, Eds.), pp. 492–580. Univ. of Arizona, Tucson.

CINTALA, M. J., S. SMREKAR, F. HÖRZ, AND F. CARDENAS (1985). Impact experiments in H_2O ice. I. Cratering (abstract). In *Lunar and Planetary Science XVI*, pp. 131–132. The Lunar and Planetary Institute, Houston, TX.

CLARK, R. N. (1982). Implications of using broadband photometry for compositional remote sensing of icy objects. *Icarus* **49,** 244–257.

CROFT, S. W. (1981). Hypervelocity impact cratering in icy media (abstract). In *Lunar and Planetary Science XII*, pp. 190–192. The Lunar and Planetary Institute, Houston, TX.

CROFT, S. W., S. W. KIEFFER, AND T. J. AHRENS (1979). Low velocity impact craters in ice and ice-saturated sand with implications for Martian crater count ages. *J. Geophys. res.* **84,** 8023–8032.

GAFFNEY, E. S., AND D. L. MATSON (1980). Water ice polymorphs and their significance on planetary surfaces. *Icarus* **44,** 511–519.

GAULT, D. E. (1973). Displaced mass, depth, diameter, and effects of oblique trajectories for impact craters formed in dense crystalline rocks. *The Moon* **6,** 32–44.

GAULT, D. E., J. E. GUEST, J. B. MURRAY, D. DZURISIN, AND M. C. MALIN (1975). Some comparisons of impact craters on Mercury and the Moon. *J. Geophys. Res.* **80,** 2444–2460.

GAULT, D. E., AND J. A. WEDEKIND (1977). Experimental hypervelocity impact into quartz sand. II. Effects of gravitational acceleration. In *Impact and Explosion Cratering* (D. Roddy *et al.*, Eds.), pp. 1231–1244. Pergamon, Elmsford, NY.

HANDIN, J. (1966). Strength and ductility. In *Handbook of Physical Constants* (S. P. Clark, Ed.), pp. 223–290. Geol. Soc. Memoir, Geol. Soc. Amer., Boulder, CO.

HOBBS, P. V. (1974). *Ice Physics*. Oxford Univ. Press (Clarendon), London/New York.

HOLSAPPLE, K. A., AND K. R. HOUSEN (1986). Cratering estimates for ice. *J. Geophys. Res.*, in press.

HOLSAPPLE, K. A., AND R. M. SCHMIDT (1982). On the scaling of crater dimensions. II. Impact processes. *J. Geophys. Res.* **87,** 1849–1870.

HÖRZ, F. (1969). Structural and mineralogical evaluation of an experimentally produced impact crater in granite. *Contrib. Mineral. Petrol.* **21,** 365–377.

HOUSEN, K. R., R. M. SCHMIDT, AND K. A. HOLSAPPLE (1983). Crater ejecta scaling laws: Fundamental forms based on dimensional analysis. *J. Geophys. Res.* **88,** 2485–2499.

KAWAKAMI, S. I., H. MIZUTANI, Y. TAKAGI, M. KATO, AND M. KUMAZAWA (1983). Impact experiments on ice. *J. Geophys. Res.* **88,** 5806–5814.

LANGE, M. A. (1985). Measurements of thermal parameters in Antarctic show and firn. *Ann. Glaciol.* **6,** 100–104.

LANGE, M. A., AND T. J. AHRENS (1981). Fragmentation of ice by low velocity impact. *Proc. Lunar and Planet. Sci. Conf. XII*, 1667–1687.

LANGE, M. A., AND T. J. AHRENS (1982a). Impact cratering in ice and ice–silicate targets: An experimental assessment (abstract). In *Lunar and Planetary Science XIII*, pp. 415–416. Lunar and Planetary Institute, Houston, TX.

LANGE, M. A., AND T. J. AHRENS (1982b). The dynamic tensile strength of ice and ice–silicate mixtures. *J. Geophys. Res.* **88,** 1197–1208.

MIZUTANI, H., S. I. KAWAKAMI, Y. TAKAGI, M. KATO, AND M. KUMAZAWA (1983). Cratering experiments in sands and a trial for general scaling law. *J. Geophys. Res.* **88,** A835–A845.

MOORE, H. J. (1976). *Missile Impact Craters (White Sands Missile Range, NM)* AND APPLICATIONS TO LUNAR RESEARCH. U.S. Geol. Surv. Prof. Pap. **812B,** p. 47.

MOORE, H. J., D. E. GAULT, AND R. V. LUGN (1963). Experimental impact craters in basalt. *Trans. Min. Eng.* **229,** 258–262.

MORRISON, D. (Ed.) (1982). *Satellites of Jupiter.* Univ. of Arizona Press, Tucson.

PARAMESWARAN, V. R., AND S. J. JONES (1975). Brittle fracture of ice at 77K. *J. Glaciol.* **14,** 305–315.

PASSEY, Q. R., AND E. M. SHOEMAKER (1982). Craters and basins on Ganymede and Callisto: Morphological indicators of crustal evolution. In *The Satellites of Jupiter* (D. Morrison, Ed.), pp. 379–434. Univ. of Arizona Press, Tucson.

RODDY, D. J., R. O. PEPIN, AND R. B. MERRILL (Eds.) (1977). *Impact and Explosion Cratering.* Pergamon, Elmsford, NY.

SHOEMAKER, E. M., B. K. LUCCHITA, J. B. PLESCIA, S. W. SQUYES, AND D. E. WILHELMS (1982). The geology of Ganymede. In *The Satellites of Jupiter* (D. Morrison, Ed.), pp. 435–520. Univ. of Arizona Press, Tucson.

SHOEMAKER, E. M., AND R. F. WOLFE (1982). Cratering timescales for the Galilean satellites. In *The Satellites of Jupiter* (D. Morrison, Ed.), pp. 277–339. Univ. of Arizona Press, Tucson.

SMITH, B. F., L. A. SODERBLOM, R. BEEBE, J. BOYCE, G. BRIGGS, A. BUNKER, S. A. COLLINS, C. F. HANSEN, T. V. JOHNSON, J. L. MITCHELL, R. J. TERRILLE, M. CARR, A. F. COOK, J. CUZZI, J. B. POLLACK, G. E. DANIELSON, A. INGERSOLL, M. E. DAVIES, G. HUNT, H. MASURSKY, E. M. SHOEMAKER, D. MORRISON, T. OWEN, C. SAGAN, J. VEVERKA, J. STROM, AND V. E. SUOMI (1981). Encounter with Saturn: Voyager 1 imaging science results. *Science* **212,** 163–191.

SMITH, B. F., L. A. SODERBLOM, R. BEEBE, J. BOYCE, G. BRIGGS, M. CARR, S. A. COLLINS, A. F. COOK, G. E. DANIELSON, M. E. DAVIES, G. E. HUNT, A. INGERSOLL, T. V. JOHNSON, J. MCCAULY, H. MASURSKY, T. OWEN, C. SAGAN, E. M. SHOEMAKER, S. STROM, V. E. SUOMI, AND J. VEVERKA (1979). The Galilean satellites and Jupiter: Voyager 2 imaging science results. *Science* **206,** 927–950.